

# Phase diagram of the Quantum Electrodynamics of 2D and 3D Dirac semimetals

J. González

*Instituto de Estructura de la Materia, Consejo Superior de Investigaciones Científicas, Serrano 123, 28006 Madrid, Spain*

(Dated: September 3, 2015)

We study the Quantum Electrodynamics of 2D and 3D Dirac semimetals by means of a self-consistent resolution of the Schwinger-Dyson equations, aiming to obtain the respective phase diagrams in terms of the relative strength of the Coulomb interaction and the number  $N$  of Dirac fermions. In this framework, 2D Dirac semimetals have just a strong-coupling instability characterized by exciton condensation (and dynamical generation of mass) that we find at a critical coupling well above previous theoretical estimates, thus explaining the absence of that instability in free-standing graphene samples. On the other hand, we show that 3D Dirac semimetals have a richer phase diagram, with a strong-coupling instability leading to dynamical mass generation up to  $N = 4$  and a line of critical points for larger values of  $N$  characterized by the vanishing of the electron quasiparticle weight in the low-energy limit. Such a critical behavior signals the transition to a strongly correlated liquid, characterized by noninteger scaling dimensions that imply the absence of a pole in the electron propagator and are the signature of non-Fermi liquid behavior with no stable electron quasiparticles.

## I. INTRODUCTION

The discovery of graphene[1] has marked the beginning of a new chapter in condensed matter physics, with the appearance of new fundamental concepts and materials with unconventional properties. We have known about other genuine 2D materials like the transition metal dichalcogenides, and we have learned about the features hidden in the band structure of the topological insulators[2, 3]. Lately, we have also seen the discovery of 3D Dirac semimetals which are the higher-dimensional analog of graphene[4–7], and we have witnessed the ongoing search of Weyl semimetals with a built-in breakdown of parity and time-reversal invariance.

In the above instances, most part of the unconventional features of the materials come from the peculiar geometrical and topological properties of the band structure. Moreover, these are electron systems that are prone to being placed in the strong coupling regime, with a large relative strength of the Coulomb interaction. Graphene should be a clear example of electron system with strong interaction, given the large ratio between the square of the electron charge and the Fermi velocity in the 2D material. However, graphene is not a prototype of strongly correlated system, even in the case of the free-standing material in vacuum, as experimental observations have shown no sign of electronic instability down to very low doping levels[8].

On the other hand, most part of theoretical studies[9–21] have estimated that 2D Dirac semimetals should have an excitonic instability at a critical point below the maximum interaction strength attained in graphene suspended in vacuum. The absence of any signature of a gap in the electronic spectrum, even below the meV scale, is certainly a puzzling evidence regarding the behavior of the 2D material. Given that the theoretical analyses have been mainly based on a ladder approximation to the electron self-energy corrections, the discrepancy between theory and experiment calls into question the use of such approximate methods in electron systems that are placed in the strong-coupling regime[22].

In this paper, we apply a nonperturbative approach to the investigation of the effects of the Coulomb interaction in both 2D and 3D semimetals, with the aim of mapping more confidently the different phases that may appear in those electron systems. More precisely, we carry out the self-consistent resolution of the Schwinger-Dyson equations for the Quantum Electrodynamics (QED) of 2D and 3D Dirac semimetals, in which the scalar part of the electromagnetic potential is used to mediate in each case the long-range  $e$ - $e$  interaction. This approach has to be implemented in general with some kind of truncation to guarantee its practical feasibility. In this regard, we have relied on a formulation of the equations that amounts to including all kinds of diagrammatic contributions except those containing vertex corrections. Nevertheless, the solutions obtained in this way account for the renormalization of all the quasiparticle parameters, giving rise to frequency and momentum-dependent forms of the quasiparticle weight, the Fermi velocity and the dynamical Dirac fermion mass.

In this framework, we will see that 2D Dirac semimetals have just a strong-coupling instability characterized by exciton condensation (and dynamical generation of mass) that we find at a critical coupling well above the estimates based on a ladder approximation, thus explaining the absence of that instability in free-standing graphene samples. On the other hand, we will show that 3D Dirac semimetals have a richer phase diagram, with a strong-coupling instability leading to dynamical mass generation up to  $N = 4$  and a line of critical points for larger values of  $N$  characterized by the vanishing of the electron quasiparticle weight in the low-energy limit[23]. We will see that such a critical behavior marks the transition to a strongly correlated liquid, characterized by noninteger scaling dimensions

that imply the absence of a pole in the electron propagator and are the signature of non-Fermi liquid behavior with no stable electron quasiparticles[24].

## II. QUANTUM ELECTRODYNAMICS OF DIRAC SEMIMETALS

We focus on the QED of Dirac semimetals, for which the Fermi velocity  $v_F$  is much smaller than the speed of light. The dynamics of these systems can be then described by the interaction of a number  $N$  of four-component Dirac spinor fields  $\psi_i(\mathbf{r})$  representing the electron quasiparticles and the scalar part  $\phi(\mathbf{r})$  of the electromagnetic potential. In principle, each spinor can represent the electronic states around a different Dirac point in momentum space, but we will not make more explicit such a discrimination as it does not play any role in the subsequent analysis. The hamiltonian can be written in general as

$$H = iv_F \int d^D r \psi_i^\dagger(\mathbf{r}) \gamma_0 \gamma \cdot \nabla \psi_i(\mathbf{r}) + e \int d^D r \psi_i^\dagger(\mathbf{r}) \psi_i(\mathbf{r}) \phi(\mathbf{r}) \quad (1)$$

where  $\{\gamma_\alpha\}$  is a set of Dirac matrices satisfying  $\{\gamma_\alpha, \gamma_\beta\} = 2\eta_{\alpha\beta}$  (with the Minkowski metric in  $D + 1$  dimensions  $\eta = \text{diag}(-1, 1, \dots, 1)$ ).

The expression (1) holds equally well for dimension  $D = 2$  and 3, but the propagator of the  $\phi$  field is very different in the two cases. The scalar field has to mediate the  $e$ - $e$  interaction with long-range Coulomb potential  $V(\mathbf{r}) = 1/|\mathbf{r}|$ , irrespective of the spatial dimension. At  $D = 2$ , this leads to a bare propagator  $D_0(\mathbf{q}, \omega)$  for the  $\phi$  field

$$D_0(\mathbf{q})|_{D=2} = \frac{1}{2|\mathbf{q}|} \quad (2)$$

while in 3D space the bare propagator is instead

$$D_0(\mathbf{q})|_{D=3} = \frac{1}{\mathbf{q}^2} \quad (3)$$

The effects of the interaction can be characterized through the corrections undergone by the scalar and the Dirac field propagators. The full Dirac propagator  $G(\mathbf{k}, \omega_k)$  has in general a representation of the form

$$G(\mathbf{k}, \omega_k)^{-1} = (\omega_k - v_F \gamma_0 \gamma \cdot \mathbf{k}) - \Sigma(\mathbf{k}, \omega_k) \quad (4)$$

in terms of a self-energy correction  $\Sigma(\mathbf{k}, \omega_k)$  that contributes to renormalize the bare quasiparticle parameters. This object is given in turn by the equation

$$i\Sigma(\mathbf{k}, \omega_k) = -e^2 \int \frac{d^D p}{(2\pi)^D} \frac{d\omega_p}{2\pi} D(\mathbf{p}, \omega_p) G(\mathbf{k} - \mathbf{p}, \omega_k - \omega_p) \Gamma(\mathbf{p}, \omega_p; \mathbf{k}, \omega_k) \quad (5)$$

where  $D(\mathbf{p}, \omega_p)$  stands for the full propagator of the scalar potential and  $\Gamma(\mathbf{q}, \omega_q; \mathbf{k}, \omega_k)$  represents the irreducible three-point vertex. More precisely, this function is defined by the expectation value

$$ie\Gamma(\mathbf{q}, \omega_q; \mathbf{k}, \omega_k) = \langle \phi(\mathbf{q}, \omega_q) \psi_i(\mathbf{k} - \mathbf{q}, \omega_k - \omega_q) \psi_i^\dagger(\mathbf{k}, \omega_k) \rangle_{1\text{PI}} \quad (6)$$

where 1PI means that we must take the irreducible part of the correlator.

Furthermore,  $D(\mathbf{p}, \omega_p)$  has also its own equation representing it in terms of the full propagators and the irreducible vertex. We can write

$$D(\mathbf{q}, \omega_q)^{-1} = D_0(\mathbf{q})^{-1} - \Pi(\mathbf{q}, \omega_q) \quad (7)$$

with the polarization  $\Pi(\mathbf{q}, \omega_q)$  being given by

$$i\Pi(\mathbf{q}, \omega_q) = Ne^2 \int \frac{d^D p}{(2\pi)^D} \frac{d\omega_p}{2\pi} \text{Tr} [G(\mathbf{q} + \mathbf{p}, \omega_q + \omega_p) \Gamma(\mathbf{q}, \omega_q; \mathbf{p}, \omega_p) G(\mathbf{p}, \omega_p)] \quad (8)$$

Moreover, the form of the irreducible vertex  $\Gamma(\mathbf{q}, \omega_q; \mathbf{k}, \omega_k)$  is constrained by the Ward identity arising from the reduced gauge invariance of the model, admitting also a representation in terms of the full propagators[25].

The expressions (5) and (8) correspond to the Schwinger-Dyson equations of the model. Together with a suitable representation of the irreducible vertex, they may lead to valuable information about the form of the full fermion and

interaction propagators. In general, however, one has to resort to some kind of truncation to achieve a self-consistent resolution of the integral equations. In what follows, we will apply a common procedure, the so-called bare vertex approximation, by which  $\Gamma(\mathbf{q}, \omega_q; \mathbf{k}, \omega_k)$  is set equal to the unit matrix in the resolution of (5) and (8). We note that this truncation does not satisfy the mentioned Ward identity, which relates the irreducible vertex to the derivative with respect to the frequency of the fermion self-energy. In this regard, the present work focuses on the investigation of dynamical effects in the renormalization of the quasiparticle parameters, which could be further improved by introducing a suitable ansatz for the vertex (in similar fashion as in the fully relativistic QED[25]). Nevertheless, we note that the relevant features reported below within our approach are consistent with the results found by means of renormalization group methods[23], which supports the present formulation. The main advantage of adopting the mentioned truncation is that it leads to a very convenient implementation of the self-consistent approach, allowing us to attain easily convergence in the recursive resolution of the Schwinger-Dyson equations.

Without the vertex corrections, (5) and (8) lead indeed to closed self-consistent equations, shown diagrammatically in Fig. 1. This representation allows us to establish a comparison with other standard approaches used to deal with many-body corrections. In particular, it becomes clear that the contributions accounted for by the diagrams in Fig. 1 have a much more comprehensive content than other approaches dealing with the RPA sum of bubble diagrams for the polarization. This makes the present computational scheme much more reliable to describe the electron system away from the weak-coupling regime, incorporating effects like the renormalization of the Fermi velocity and the quasiparticle weight which are essential to capture the different critical points of the Dirac semimetals.

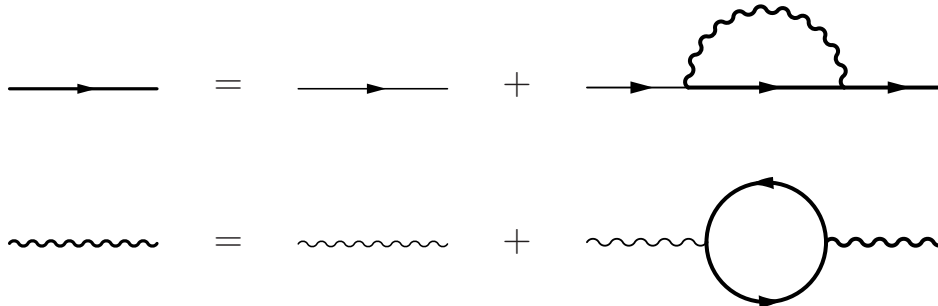


FIG. 1: Diagrammatic representation of the Schwinger-Dyson equations (in the bare vertex approximation). The thick(thin) straight line represents the dressed(free) Dirac fermion propagator and the thick(thin) wiggly line represents the dressed(undressed) interaction propagator.

### III. SELF-CONSISTENT RESOLUTION OF SCHWINGER-DYSON EQUATIONS

The integral equations represented in Fig. 1 can be solved numerically by applying a recursive procedure, after rotating first all the frequencies in the complex plane,  $\bar{\omega} = -i\omega$ , to make the passage to a Euclidean space in the variables  $(\bar{\omega}, \mathbf{k})$ . In practice, the integrals can be done numerically by discretizing the frequency and momentum variables. By choosing a set of frequencies  $\bar{\omega} = \pi(2n+1)T$  with  $n = 0, \pm 1, \pm 2, \dots$ , we can interpret such a discretization as the result of placing the theory at finite temperature  $T$ . On the other hand, computing with a grid in momentum space is equivalent to describing a system with finite spatial size. In this case, we can check the finite-size scaling of the results in order to extrapolate the behavior over large distances.

For the self-consistent resolution, it becomes convenient to represent the fermion propagator in terms of renormalization factors  $z_\psi(\mathbf{k}, i\bar{\omega})$  for the electron wave-function and  $z_v(\mathbf{k}, i\bar{\omega})$  for the Fermi velocity, adding moreover another factor  $z_m(\mathbf{k}, i\bar{\omega})$  to allow for the dynamical generation of a mass for the Dirac fermions. Thus we write the full Dirac propagator in the form

$$G(\mathbf{k}, i\bar{\omega}) = (z_\psi(\mathbf{k}, i\bar{\omega})i\bar{\omega} - z_v(\mathbf{k}, i\bar{\omega})v_F\gamma_0\boldsymbol{\gamma} \cdot \mathbf{k} - z_m(\mathbf{k}, i\bar{\omega})\gamma_0)^{-1} \quad (9)$$

In this way, the resolution consists in finding the functions  $z_\psi(\mathbf{k}, i\bar{\omega})$ ,  $z_v(\mathbf{k}, i\bar{\omega})$  and  $z_m(\mathbf{k}, i\bar{\omega})$  that attain the self-consistency in the Schwinger-Dyson equations.

One more important detail is that the polarization  $\Pi(\mathbf{q}, \omega_q)$  may develop spurious divergences when computing the momentum integrals with a simple cutoff  $\Lambda_k$ . In general, only a gauge-invariant regularization scheme can produce results without non-physical power-law dependences on the cutoff[26]. These are anyhow additive contributions to the polarization, which makes possible to get rid of them by a suitable subtraction procedure. Thus, computing with

the momentum cutoff, the polarization at  $D = 2$  shows a contribution proportional to  $\Lambda_k$ , while the corresponding function at  $D = 3$  has terms growing as large as  $\Lambda_k^2$ . In our self-consistent resolution, we have carried out the frequency integrals first with a cutoff  $\Lambda \gg v_F \Lambda_k$ , implementing afterwards the subtraction procedure to remove the power-law dependences on  $\Lambda_k$  from the polarization. In this way, we have ended up with expressions of  $\Pi(\mathbf{q}, \omega_q)$  that are functionals of the renormalization factors, displaying leading behaviors at small  $\mathbf{q}$  proportional to  $|\mathbf{q}|$  and  $\mathbf{q}^2$ , respectively, for  $D = 2$  and  $D = 3$ .

### A. 2D Dirac semimetals

Solving the Schwinger-Dyson equations at  $D = 2$ , we find in general that the function  $z_\psi(\mathbf{k}, i\bar{\omega})$  giving the quasiparticle weight remains bounded, while  $z_v(\mathbf{k}, i\bar{\omega})$  diverges in the limit of small momentum  $\mathbf{k} \rightarrow 0$ . As long as the effective Fermi velocity depends on the momentum scale, it is convenient to define the bare value  $v_B = z_v(\Lambda_k, 0)v_F$ , which can be taken as a good measure of the Fermi velocity at the microscopic scale (it is always verified that  $z_\psi(\Lambda_k, 0) \approx 1$ ). We can then define the unrenormalized coupling giving the bare interaction strength as

$$\alpha = e^2/4\pi v_B \quad (10)$$

which can take different values depending on the particular Fermi velocities of the 2D Dirac semimetals.

As an illustration of the general behavior, Fig. 2 represents the solution obtained for  $z_\psi(\mathbf{k}, i\bar{\omega})$  and  $z_v(\mathbf{k}, i\bar{\omega})$  for  $N = 2$  and  $\alpha = 2.2$ , that is, for parameters that should be appropriate to describe graphene samples suspended in vacuum. The resolution has been carried out taking a discretization of the frequency variables such that  $2\pi T \approx 0.01$  eV. In this case, the self-consistency in the equations is only attained when  $z_m(\mathbf{k}, i\bar{\omega})$  is set identically equal to zero. The behavior found for  $z_\psi(\mathbf{k}, i\bar{\omega})$  and  $z_v(\mathbf{k}, i\bar{\omega})$  is in agreement with the general trend obtained from renormalization group methods, which found the divergence of the Fermi velocity in the low-energy limit as a most relevant feature[26, 27].

For comparison, we have also represented in Fig. 2 the dependence on the energy scale  $\varepsilon$  of the inverse of the quasiparticle weight  $z(\varepsilon)$  and the renormalized Fermi velocity  $v(\varepsilon)$  obtained from the renormalization group approach in the large- $N$  approximation[27]. It can be observed anyhow that the plot of  $z_v(\mathbf{k}, 0)/z_\psi(\mathbf{k}, 0)$  (full line in Fig. 2(b)) follows the experimental results of Ref. 8 (Fig. 2(c) in that paper) much more accurately than the scale dependence of the Fermi velocity obtained with the renormalization group method in the large- $N$  approximation (dashed line in Fig. 2(b))[28].

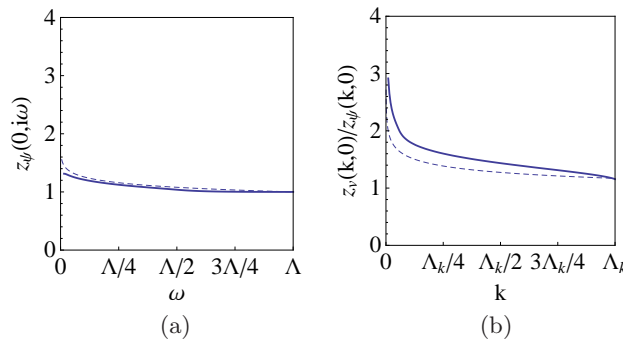


FIG. 2: Plot of the factors  $z_\psi(0, i\omega)$  and  $z_v(\mathbf{k}, 0)/z_\psi(\mathbf{k}, 0)$  (full lines in (a) and (b)) for a 2D Dirac semimetal with  $N = 2$ , bare coupling  $\alpha = 2.2$ , and  $2\pi T \approx 0.01$  eV. The dashed lines represent the dependence on the energy scale  $\varepsilon$  of the inverse of the quasiparticle weight  $z(\varepsilon)$  (in (a)) and the renormalized Fermi velocity  $v(\varepsilon)$  (in (b)) obtained with the renormalization group approach for the same bare coupling in the large- $N$  approximation.

With our nonperturbative approach, moreover, we can ask whether the tendency towards a noninteracting Fermi liquid, implied by the growth of the Fermi velocity, can be arrested by some instability as the bare coupling  $\alpha$  is increased. The outcome of this search is that the other relevant feature of the 2D Dirac semimetals is the development of a nonvanishing mass  $z_m(\mathbf{k}, i\bar{\omega})$  at sufficiently large interaction strength, as illustrated in Fig. 3. This corresponds to the onset of a phase with chiral symmetry breaking and dynamical generation of a gap for the Dirac fermions, as predicted by several other methods[9–21].

We observe that the divergence of  $z_v$  in the low-energy limit does not prevent the development of a nonvanishing dynamical mass  $z_m$ , while  $z_\psi$  remains finite across the transition. This latter fact implies that chiral symmetry breaking proceeds without an anomalous scaling of the Dirac fermion field, in agreement with field theory studies of

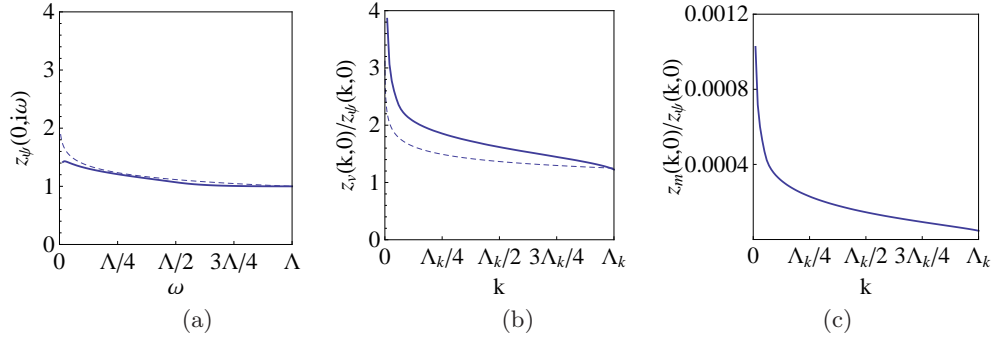


FIG. 3: Plot of  $z_\psi(0, i\omega)$ ,  $z_v(\mathbf{k}, 0)/z_\psi(\mathbf{k}, 0)$ , and  $z_m(\mathbf{k}, 0)/z_\psi(\mathbf{k}, 0)$  measured in eV (full lines in (a), (b) and (c)) for a 2D Dirac semimetal with  $N = 2$ , bare coupling  $\alpha = 3.37$ , and  $2\pi T \approx 0.01$  eV. The dashed lines represent the dependence on the energy scale  $\varepsilon$  of the inverse of the quasiparticle weight  $z(\varepsilon)$  (in (a)) and the renormalized Fermi velocity  $v(\varepsilon)$  (in (b)) obtained with the renormalization group approach for the same bare coupling in the large- $N$  approximation.

that phenomenon[29]. In general, we also expect that the divergent growth of the Fermi velocity is arrested at the energy scale for which the quasiparticle dispersion becomes gapped (which is not appreciated in the case of Fig. 3(b) as the infrared cutoff set in that plot by finite-size effects is slightly above 1 meV).

The present approach has the virtue of allowing an accurate determination of the critical coupling  $\alpha_c$  for the transition to the broken symmetry phase. We have represented in Fig. 4 the plot of the critical coupling obtained as a function of  $N$ , which leads to a map of the two different phases in the QED of the 2D Dirac semimetals. In agreement with earlier analyses, we observe that  $\alpha_c$  turns out to grow with  $N$ , though in the present resolution there seems to be no upper limit in the number of Dirac fermions for the development of the transition[30]. We have also checked that the approach to the critical coupling seems to be consistent with a transition of infinite order, since the dynamical mass exhibits an inflection point as a function of coupling constant above  $\alpha_c$  which is the signature of that kind of transition under finite-size effects[31].

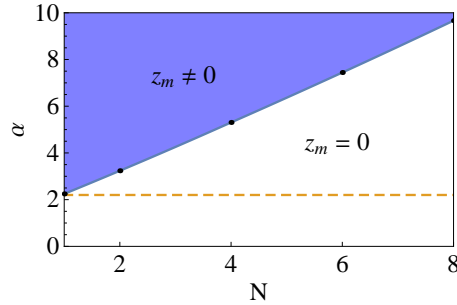


FIG. 4: Phase diagram of the QED of 2D Dirac semimetals showing the region with dynamically generated fermion mass  $z_m \neq 0$ . The critical line has been obtained from the self-consistent resolution of the Schwinger-Dyson equations with  $2\pi T \approx 0.01$  eV. The dashed line marks the nominal interaction strength  $\alpha \approx 2.2$  corresponding to graphene suspended in vacuum.

In any case, the most relevant result regarding the phase diagram in Fig. 4 is that the point corresponding to real graphene samples suspended in vacuum falls in the region with no dynamical generation of mass. For the number  $N = 2$  of Dirac fermions in graphene, the critical coupling obtained for chiral symmetry breaking turns out to be indeed well above most part of previous estimates relying on a restricted sum of many-body corrections. The present results explain therefore that no gap has been found in the electronic spectrum of graphene, even in experiments looking very close to the Dirac point[8]. The reason for the unexpectedly large values of the critical coupling can be traced back to the combination of the slight suppression of the quasiparticle weight and the large growth of the Fermi velocity at low energies[32]. These two effects cooperate to reduce significantly the effective strength of the Coulomb interaction for the development of the gap, stressing the importance of a proper account of all the renormalization factors for the accurate determination of the transition to the broken symmetry phase.

### B. 3D Dirac semimetals

The 3D Dirac semimetals have in general a number of Dirac points that have attached (each of them) fermions with the two different chiralities. This is in particular the case of materials recently discovered like  $\text{Na}_3\text{Bi}$  and  $\text{Cd}_3\text{As}_2$ , as already clarified by their theoretical analysis[33, 34]. Such a distinctive feature of the 3D Dirac semimetals is relevant in the present study, since it makes possible the dynamical generation of mass and opening of a gap in these systems from the hybridization of two chiralities at the same Dirac point.

More precisely, the low-energy electronic states in both  $\text{Na}_3\text{Bi}$  and  $\text{Cd}_3\text{As}_2$  can be naturally arranged into four-component spinors around each of two Dirac points, in such a way that the Dirac matrices appear in the chiral representation

$$\gamma_0 \gamma_i = \eta_i \begin{pmatrix} \sigma_i & 0 \\ 0 & -\sigma_i \end{pmatrix} \quad (11)$$

with  $\eta_1 = \eta_2 = 1$  and  $\eta_3 = \pm 1$  depending on the Dirac point. The dynamical mass generation that we impose with the ansatz (9) corresponds in this scheme to the mixing of the two chiralities, realized by the Dirac matrix

$$\gamma_0 = \begin{pmatrix} 0 & -\mathbb{1} \\ -\mathbb{1} & 0 \end{pmatrix} \quad (12)$$

A term proportional to (12) has been identified in Refs. [33] and [34] as one of the possible perturbations of the Dirac hamiltonian in  $\text{Na}_3\text{Bi}$  and  $\text{Cd}_3\text{As}_2$ . The physical meaning of such a term has to be found in the breakdown of the threefold and fourfold rotational symmetry in each case, having an effect similar to that induced by strain in the crystal lattice.

The dynamical mass generation we are discussing corresponds then to the development of an expectation value

$$\langle \psi_i^\dagger \gamma_0 \psi_i \rangle \neq 0 \quad (13)$$

within each Dirac point  $i$ . We can imagine nevertheless the possibility of a symmetry breaking pattern with order parameter given by

$$\langle \psi_i^\dagger M \psi_j \rangle \neq 0 \quad (14)$$

with a suitable matrix  $M$  and a pair of Dirac points  $i \neq j$  [35]. Such a condensation has the feature of involving a finite momentum  $\mathbf{Q}$ , needed to connect different Dirac points. This can be pictured diagrammatically, as the order parameters (13) and (14) can be characterized in terms of the respective three-point vertices in Fig. 5. The point is that, as implied by the renormalization group approach in Ref. [36] for the 2D case, one has to hybridize the two chiralities at the same Dirac point so that the long-range Coulomb interaction may induce the strongest scaling of the three-point vertex, leading eventually to the condensation signaled by (13). The vertex in Fig. 5(b) is built from spinors at different Dirac points, which will not map in general onto each other upon a rigid shift by the momentum  $\mathbf{Q}$  and may lead therefore to a weaker overlap. This means that, for a generic 3D Dirac semimetal with long-range Coulomb interaction, the maximum strength will be set by the vertex in Fig. 5(a), ensuring at least the condensation given by (13) whenever symmetry breaking is to take place in the system.

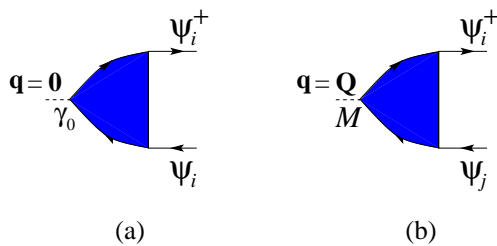


FIG. 5: Diagrammatic representation of the three-point vertices involving the composite operators  $\psi_i^\dagger \gamma_0 \psi_i$  and  $\psi_i^\dagger M \psi_j$ , with respective momentum transfer  $\mathbf{q} = 0$  and  $\mathbf{q} = \mathbf{Q}$  connecting Dirac points.

Apart from the phenomenon of dynamical mass generation, the 3D Dirac semimetals have a tendency to develop at strong coupling a drastic attenuation of the quasiparticle weight at low energies, with a much softer renormalization



of the Fermi velocity in comparison to their 2D Dirac analogues[37]. This behavior has been already found in an analytic study of the 3D electron systems in the large- $N$  limit, where it has been possible to establish rigorously the existence of a critical coupling at which the quasiparticle weight vanishes in the low-energy limit[23]. In Fig. 6 we can see the effect of the critical behavior in the functions  $z_\psi(\mathbf{k}, i\bar{\omega})$  and  $z_v(\mathbf{k}, i\bar{\omega})$ , computed in the present approach for  $N = 6$  close to the critical point and with a discretization such that  $2\pi T \approx 0.02$  eV. For smaller values of  $N$ , we will see that there is however an interplay between that quasiparticle attenuation and the tendency to dynamical generation of mass. For  $N \leq 4$ , this latter effect becomes actually dominant, leading to a phase with chiral symmetry breaking that is the analog of the broken symmetry phase found in the 2D Dirac semimetals[38].

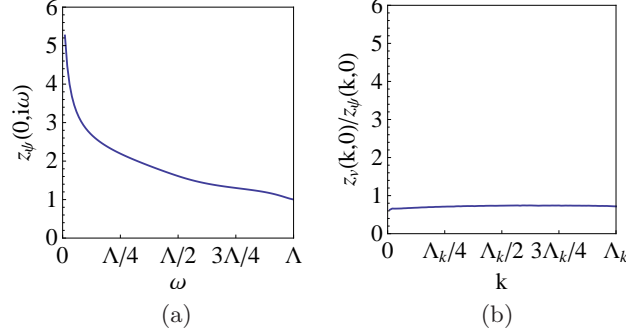


FIG. 6: Plot of the factors  $z_\psi(0, i\omega)$  and  $z_v(\mathbf{k}, 0)/z_\psi(\mathbf{k}, 0)$  for a 3D Dirac semimetal with  $N = 6$ , bare coupling  $g = 36.8$ , and  $2\pi T \approx 0.02$  eV.

From the self-consistent resolution of the Schwinger-Dyson equations, we have determined for each value of  $N$  the critical coupling at which the electron system becomes first unstable, either from the vanishing of the quasiparticle weight or from the dynamical generation of a gap. In the case of the 3D Dirac semimetals, one has to take special care to refer the parameters to a given scale, since quantities like the electron charge and the Fermi velocity are renormalized at low energies. In this respect, we have chosen to define the bare electron charge  $e_B$  at the highest value of the momentum cutoff, according to the relation  $e_B^2 = \Lambda_k^2 D(\Lambda_k, 0) e^2$ . Then, we can take for the microscopic parameter  $e_B$  the standard value of the electron charge. As in the case of the 2D Dirac semimetals, we have also defined the bare Fermi velocity by  $v_B = z_v(\Lambda_k, 0) v_F$ . Thus, we have computed all the critical couplings referred to the relative interaction strength at the microscopic scale, given by

$$g = N e_B^2 / 4\pi v_B \quad (15)$$

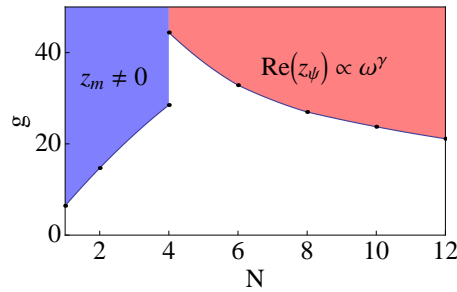


FIG. 7: Phase diagram of the QED of 3D Dirac semimetals, showing the region with dynamical generation of mass ( $z_m \neq 0$ ) and the region corresponding to non-Fermi liquid behavior (with  $\text{Re}(z_\psi(0, i\omega)) \propto \omega^\gamma$ ,  $\gamma < 0$ ). The critical lines have been obtained from the self-consistent resolution of the Schwinger-Dyson equations with  $2\pi T \approx 0.02$  eV.

The results we have obtained are condensed in the phase diagram shown in Fig. 7. We observe that there is always a phase connected to weak coupling for all values of  $N$ , characterized by a gapless spectrum of quasiparticles whose parameters remain regular at low energies. This phase terminates for  $N \leq 4$  in the dynamical generation of a fermion mass at sufficiently strong coupling, which in our approach is reflected in the onset of a nonvanishing  $z_m(\mathbf{k}, i\bar{\omega})$ . This is shown in Fig. 8, where we have represented the different renormalization factors for  $N = 2$  at a coupling above the critical point. For this value of  $N$ , we observe that the renormalization of the quasiparticle weight is a moderate

effect as the gap opens up in the electronic spectrum. This soft behavior has been also observed in the studies of dynamical mass generation in the fully relativistic QED, carried out by means of the self-consistent resolution of the corresponding Schwinger-Dyson equations[25].

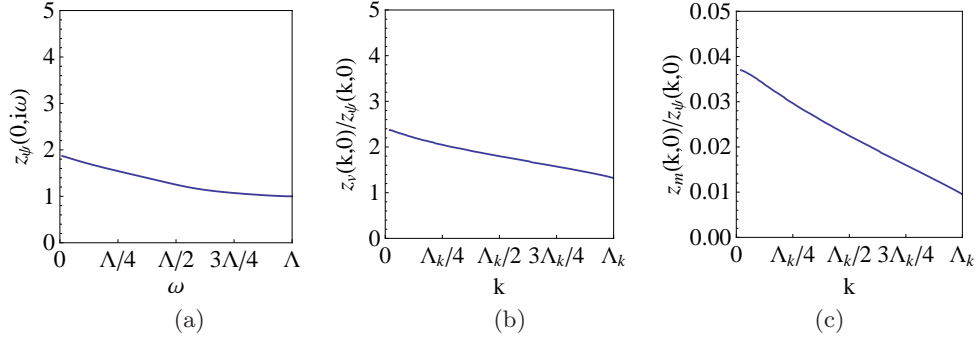


FIG. 8: Plot of the factors  $z_\psi(0, i\omega)$ ,  $z_v(\mathbf{k}, 0)/z_\psi(\mathbf{k}, 0)$  and  $z_m(\mathbf{k}, 0)/z_\psi(\mathbf{k}, 0)$  (measured in eV) for a 3D Dirac semimetal with  $N = 2$ , bare coupling  $g = 15.1$ , and  $2\pi T \approx 0.02$  eV.

The case of  $N = 4$  is however specially interesting, since there is then an interplay between the dynamical generation of mass and the strong attenuation of the quasiparticle weight. This can be observed in Fig. 9, where we have plotted  $z_\psi(\mathbf{k}, i\bar{\omega})$ ,  $z_v(\mathbf{k}, i\bar{\omega})$  and  $z_m(\mathbf{k}, i\bar{\omega})$  for different couplings below and above the point where the mass develops. We see that, while the breakdown of chiral symmetry takes place before the system is completely destabilized by the large growth of  $z_\psi(\mathbf{k}, i\bar{\omega})$ , this latter effect may still have a large impact on the observation of the quasiparticles in the electron system.

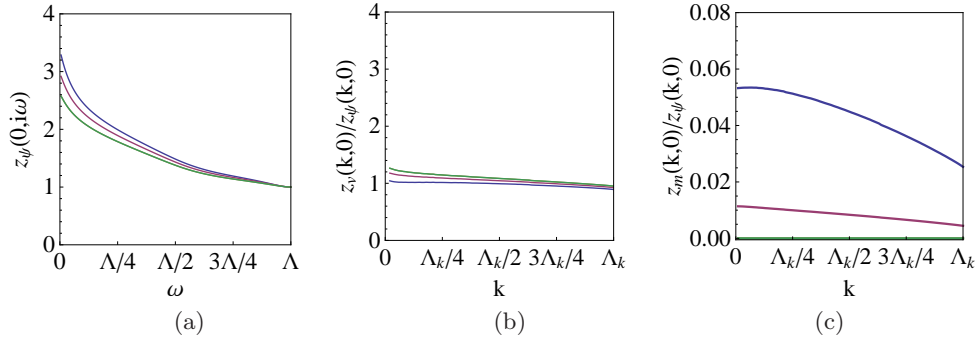


FIG. 9: Plot of the factors  $z_\psi(0, i\omega)$ ,  $z_v(\mathbf{k}, 0)/z_\psi(\mathbf{k}, 0)$  and  $z_m(\mathbf{k}, 0)/z_\psi(\mathbf{k}, 0)$  (in eV) for a 3D Dirac semimetal with  $N = 4$ , bare coupling  $g = 30.1, 27.6, 24.9$  (from top to bottom in (a) and (c), from bottom to top in (b)), and  $2\pi T \approx 0.01$  eV.

On the other hand, we find that for  $N > 4$  there is always a critical coupling at which the divergence of  $z_\psi(0, i\omega)$  takes place before the dynamical generation of mass, according to the trend illustrated in Fig. 6. The present approach allows us moreover to investigate the phase of the electron system above the critical point. The self-consistent resolution of the Schwinger-Dyson equations gives rise in that case to renormalization factors that get in general an imaginary part, as shown in Fig. 10. This has to be interpreted as the signature of a nonperturbative instability of the electron quasiparticles since, in the conventional perturbative approach, the self-energy corrections obtained after Wick rotation  $\omega = i\bar{\omega}$  can only account for the renormalization of the real part of the quasiparticle parameters. In our approach, the divergence of the imaginary part of  $z_\psi(0, i\bar{\omega})$  at  $\bar{\omega} = 0$  points actually to the development of a strongly correlated liquid, which is confirmed by the concomitant suppression of the quasiparticle weight in the low-energy limit, observed in the plots of Fig. 10.

A detailed analysis of the renormalization factor  $z_\psi(0, i\bar{\omega})$  in Fig. 10 reveals indeed that the real part of such a function follows accurately a power-law behavior as  $\bar{\omega} \rightarrow 0$ . This can be clearly seen in the plots of Fig. 11, where  $\bar{\omega} \text{Re}(z_\psi(0, i\bar{\omega}))$  is represented in linear and logarithmic scale. The fit to the power-law dependence

$$\bar{\omega} \text{Re}(z_\psi(0, i\bar{\omega})) \propto \bar{\omega}^\mu \quad (16)$$



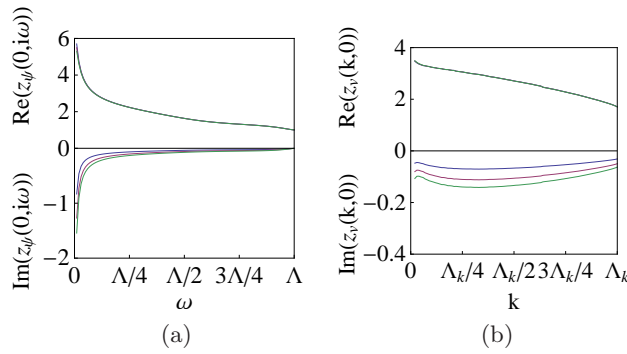


FIG. 10: Plot of the real and imaginary parts of the factors  $z_\psi(0, i\omega)$  and  $z_v(\mathbf{k}, 0)$  for a 3D Dirac semimetal with  $N = 6$ , bare coupling  $g = 37.2, 37.4, 37.6$  (from lower to higher absolute value in both sides of the plot), and  $2\pi T \approx 0.02$  eV.

gives an exponent  $\mu \approx 0.7$ , with little variation between the three curves for the different couplings. Equivalently, this corresponds to having a nonvanishing anomalous dimension of the Dirac fermion field with a value of  $\approx 0.3$ . The inspection of the renormalization of  $v_F$ , dictated by the function  $\text{Re}(z_v(\mathbf{k}, 0))/\text{Re}(z_\psi(\mathbf{k}, 0))$ , leads in this case to a picture very similar to that in Fig. 6(b). This shows that  $\mu$  corresponds to the exponent governing both the frequency and momentum scaling of the electron propagator (implying therefore a dynamical critical exponent equal to 1).

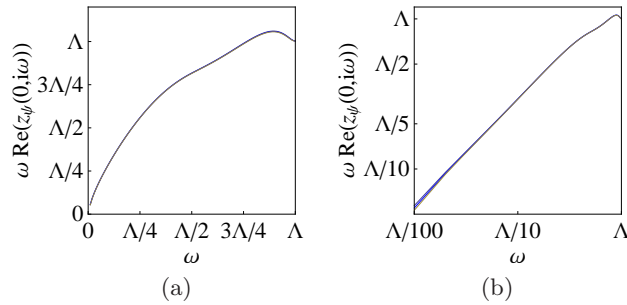


FIG. 11: Plot of  $\omega \text{Re}(z_\psi(0, i\omega))$  for a 3D Dirac semimetal with the same parameters as in Fig. 10, with (a) linear and (b) logarithmic scale (with the three different curves virtually collapsed onto the same line).

From the physical point of view, the main consequence of the noninteger exponent  $\mu$  is the absence of a pole in the electron propagator, which reflects the lack of low-energy fermion excitations. This is characteristic of correlated systems in low dimensions, where the interactions may drive into a non-Fermi liquid phase with nontrivial scaling exponents[39–43]. Our system provides in this respect an example of such a behavior at  $D = 3$ , illustrating moreover the transition to the strongly correlated phase from the renormalized Fermi liquid, which is the phase of 3D Dirac semimetals at sufficiently weak coupling.

#### IV. CONCLUSION

We have seen that the behavior of 2D and 3D Dirac semimetals is governed by quite different effects in their respective strong-coupling regimes. In our approach to the 2D semimetals, there is in general a tendency of the Fermi velocity of quasiparticles to grow large in the low-energy limit, in agreement with the renormalization group studies carried out in the large- $N$  approximation[27]. In the case of the 3D Dirac semimetals, we observe instead that the electron system is prone to develop an attenuation of the quasiparticle weight, with a less significant renormalization of the Fermi velocity. This tendency has been also identified in the large- $N$  limit of the 3D Dirac semimetals, which shows the existence of a critical coupling characterized by the divergence of the electron scaling dimension[23].

In the 2D Dirac semimetals, the divergence of the Fermi velocity in the low-energy limit is the dominant feature that explains for instance the absence of significant correlation effects in the graphene layer. Our nonperturbative solution of the Schwinger-Dyson equations incorporates naturally the scaling of the Fermi velocity, allowing us to reach very good agreement with the experimental measures from graphene samples at very low doping levels[8]. As a

result of such a renormalization, we have found that the interaction strength has to be set to relatively large values, above those attained in the suspended graphene samples, in order to open up a phase with exciton condensation and dynamical generation of a gap in the 2D Dirac semimetals.

The picture changes into a richer phase diagram for the 3D Dirac semimetals, as a consequence of the interplay between the attenuation of the electron quasiparticles that prevails at large  $N$  and the tendency to dynamical mass generation (analogous to the chiral symmetry breaking of the fully relativistic QED[44–51]) that is dominant at small  $N$ . Both effects seem to coexist at the interface found for a number of Dirac fermions  $N = 4$ . Most interestingly, our self-consistent resolution has also revealed the phase of the system above the large- $N$  critical point, allowing us to characterize the properties of a strongly correlated liquid that is reminiscent of other systems with suppression of electron quasiparticles making the transition from marginal Fermi liquid[39] to non-Fermi liquid behavior[40–43].

We remark that our analysis of the 3D Dirac semimetals can be extended to map also the large- $N$  regime of 3D Weyl semimetals. These are a class of semimetals in which a number of Weyl points host fermions with a given chirality, represented in terms of two-component spinors. This means that a self-consistent resolution of the Schwinger-Dyson equations may be also carried out for these systems, writing now the full propagator of the Weyl fermions around a given Weyl point as

$$G(\mathbf{k}, i\bar{\omega}) = (z_\psi(\mathbf{k}, i\bar{\omega})i\bar{\omega} - z_v(\mathbf{k}, i\bar{\omega})v_F\boldsymbol{\sigma} \cdot \mathbf{k})^{-1} \quad (17)$$

We may parallel the above approach to predict the existence of a phase with suppression of electron quasiparticles, similar to that found for the 3D Dirac semimetals and covering the right part of the phase diagram in Fig. 7. At small  $N$  (taken now as the number of pairs of Weyl points), a strong-coupling phase corresponding to fermion condensation may also arise, with an order parameter mixing fermions at different Weyl points as in (14). The strength of this instability cannot be assessed generically, however, since it may be highly dependent on the particular overlapping of spinors from different Weyl points. Nevertheless, we may expect a strong-coupling symmetry broken phase for 3D Weyl semimetals at small  $N$ , with a phase boundary determined by the particular form of the spinors in the material hosting the Weyl points.

We finally comment on the feasibility to observe the strong-coupling phases of the 3D semimetals, according to the values of the Fermi velocity and number of Dirac or Weyl points found in different materials. We recall in this regard that the best known examples of 3D Dirac semimetals ( $\text{Na}_3\text{Bi}$  and  $\text{Cd}_3\text{As}_2$ ) have a number  $N = 2$  of Dirac fermions and Fermi velocities that have been measured with certain accuracy[4, 52]. The quasiparticle dispersion shows in both cases an anisotropy that is reflected in the values of  $v_F$ , which may be reduced by a factor of  $\sim 4$  in one of the directions in momentum space[53]. We can make conservative estimates of the coupling defined in (15) by taking the largest Fermi velocity in each case, with the result that  $g \sim 10$  for  $\text{Na}_3\text{Bi}$  and  $g \sim 3$  for  $\text{Cd}_3\text{As}_2$ . These couplings turn out to be below the critical coupling for dynamical mass generation, which corresponds to the critical point at  $g^* \approx 14.7$  for  $N = 2$  in the phase diagram of Fig. 7. This places the two mentioned 3D Dirac semimetals in the gapless phase, showing that the transition to the regime with dynamical mass generation would require a Fermi velocity at least about 50% smaller than the largest value in  $\text{Na}_3\text{Bi}$ .

On the other hand, there should be good prospects to observe the strong-coupling phase at large  $N$  in Weyl semimetals. The most promising candidates for this class are the pyrochlore iridates and TaAs, which have 12 pairs of Weyl points. With the value of the Fermi velocity measured for TaAs[54], the large value of  $N$  already sets the effective coupling  $g$  for this material well above the critical coupling for the non-Fermi liquid regime, which is at  $g^* \approx 21.1$  for  $N = 12$ . This leads us to expect that such a material should not behave as a regular Fermi liquid when observed at filling levels sufficiently close to the Weyl points. In general, we conclude that the strong-coupling phases that we have studied in this paper are not beyond reach, and that they may be found in systems with reasonably low Fermi velocities, or with a sufficiently large number of Dirac or Weyl points already exhibited by several materials.

We acknowledge the financial support from MICINN (Spain) through grant FIS2011-23713 and from MINECO (Spain) through grant FIS2014-57432-P.

- 
- [1] K. S. Novoselov, A. K. Geim, S. V. Morozov, D. Jiang, Y. Zhang, S. V. Dubonos, I. V. Grigorieva, and A. A. Firsov, *Science* **306**, 666 (2004).
  - [2] M. Z. Hasan and C. L. Kane, *Rev. Mod. Phys.* **82**, 3045 (2010).
  - [3] X.-L. Qi and S.-C. Zhang, *Rev. Mod. Phys.* **83**, 1057 (2011).
  - [4] Z. K. Liu, B. Zhou, Y. Zhang, Z. J. Wang, H. M. Weng, D. Prabhakaran, S.-K. Mo, Z. X. Shen, Z. Fang, X. Dai, Z. Hussain and Y. L. Chen, *Science* **343**, 864 (2014).
  - [5] M. Neupane, S. Xu, R. Sankar, N. Alidoust, G. Bian, C. Liu, I. Belopolski, T.-R. Chang, H.-T. Jeng, H. Lin, A. Bansil, F. Chou and M. Z. Hasan, *Nature Commun.* **5**, 3786 (2014).

- [6] S. Borisenko, Q. Gibson, D. Evtushinsky, V. Zabolotnyy, B. Büchner and R. J. Cava, *Phys. Rev. Lett.* **113**, 027603 (2014).
- [7] S.-Y. Xu, C. Liu, S. K. Kushwaha, T.-R. Chang, J. W. Krizan, R. Sankar, C. M. Polley, J. Adell, T. Balasubramanian, K. Miyamoto, N. Alidoust, G. Bian, M. Neupane, I. Belopolski, H.-T. Jeng, C.-Y. Huang, W.-F. Tsai, H. Lin, F. C. Chou, T. Okuda, A. Bansil, R. J. Cava and M. Z. Hasan, report arXiv:1312.7624.
- [8] D. C. Elias, R. V. Gorbachev, A. S. Mayorov, S. V. Morozov, A. A. Zhukov, P. Blake, L. A. Ponomarenko, I. V. Grigorieva, K. S. Novoselov, F. Guinea and A. K. Geim, *Nature Phys.* **7**, 701 (2011).
- [9] D. V. Khvashchenko, *Phys. Rev. Lett.* **87**, 246802 (2001).
- [10] E. V. Gorbar, V. P. Gusynin, V. A. Miransky and I. A. Shovkovy, *Phys. Rev. B* **66**, 045108 (2002).
- [11] O. Vafek and M. J. Case, *Phys. Rev. B* **77**, 033410 (2008).
- [12] D. V. Khvashchenko, *J. Phys.: Condens. Matter* **21**, 075303 (2009).
- [13] I. F. Herbut, V. Juričić and O. Vafek, *Phys. Rev. B* **80**, 075432 (2009).
- [14] V. Juričić, I. F. Herbut and G. W. Semenoff, *Phys. Rev. B* **80**, 081405 (2009).
- [15] J. E. Drut and T. A. Lähde, *Phys. Rev. Lett.* **102**, 026802 (2009).
- [16] W. Armour, S. Hands and C. Strouthos, *Phys. Rev. B* **81**, 125105 (2010).
- [17] O. V. Gamayun, E. V. Gorbar and V. P. Gusynin, *Phys. Rev. B* **80**, 165429 (2009).
- [18] J. Wang, H. A. Fertig and G. Murthy, *Phys. Rev. Lett.* **104**, 186401 (2010).
- [19] O. V. Gamayun, E. V. Gorbar and V. P. Gusynin, *Phys. Rev. B* **81**, 075429 (2010).
- [20] J. Sabio, F. Sols and F. Guinea, *Phys. Rev. B* **82**, 121413(R) (2010).
- [21] J. González, *Phys. Rev. B* **85**, 085420 (2012).
- [22] This matter has been also addressed recently by J. Hofmann, E. Barnes and S. Das Sarma, *Phys. Rev. Lett.* **113**, 105502 (2014).
- [23] J. González, *Phys. Rev. B* **90**, 121107(R) (2014).
- [24] Signatures of the breakdown of the Fermi liquid picture have been also found in the 3D Dirac semimetals by J. Hofmann, E. Barnes and S. Das Sarma, *Phys. Rev. B* **92**, 045104 (2015).
- [25] J. C. R. Bloch, report arXiv:hep-ph/0208074 (Ph. D. thesis) and references therein.
- [26] J. González, F. Guinea and M. A. H. Vozmediano, *Nucl. Phys. B* **424**, 595 (1994).
- [27] J. González, F. Guinea and M. A. H. Vozmediano, *Phys. Rev. B* **59**, R2474 (1999).
- [28] In the nonrelativistic approximation, the Fermi velocity diverges without bound in the low-energy limit as a consequence of dealing with the static scalar interaction, since it has been shown in Ref. [26] that  $v(\varepsilon)$  actually converges to the speed of light in the theory with the full (retarded) gauge interaction.
- [29] D. J. Gross and A. Neveu, *Phys. Rev. D* **10**, 3235 (1974).
- [30] This feature is also present in the refined resolution of the gap equation with dynamical screening carried out in Ref. 19.
- [31] K. Y. Szeto and G. Dresselhaus, *Phys. Rev. B* **32**, 3142 (1985).
- [32] The negative effect of the Fermi velocity renormalization on the dynamical mass generation in 2D Dirac semimetals has been also stressed in Refs. 20 and 21, and by C. Popovici, C. S. Fischer and L. von Smekal, *Phys. Rev. B* **88**, 205429 (2013).
- [33] Z. Wang, Y. Sun, X.-Q. Chen, C. Franchini, G. Xu, H. Weng, X. Dai and Z. Fang, *Phys. Rev. B* **85**, 195320 (2012).
- [34] Z. Wang, H. Weng, Q. Wu, X. Dai and Z. Fang, *Phys. Rev. B* **88**, 125427 (2013).
- [35] R.-X. Zhang, J. A. Hutasoit, Y. Sun, B. Yan, C. Xu, and C.-X. Liu, report arXiv:1503.00358.
- [36] J. González, *JHEP* **08**, 27 (2012).
- [37] This scaling of the Fermi velocity in 3D Dirac semimetals has been pointed out by P. Hosur, S. A. Parameswaran, and A. Vishwanath, *Phys. Rev. Lett.* **108**, 046602 (2012), and also by B. Rosenstein and M. Lewkowicz, *Phys. Rev. B* **88**, 045108 (2013).
- [38] This phase has been also studied recently in 3D Dirac semimetals by A. Sekine and K. Nomura, *Phys. Rev. B* **90**, 075137 (2014).
- [39] C. M. Varma, P. B. Littlewood, S. Schmitt-Rink, E. Abrahams and A. E. Ruckenstein, *Phys. Rev. Lett.* **63**, 1996 (1989).
- [40] P.-A. Bares and X. G. Wen, *Phys. Rev. B* **48**, 8636 (1993).
- [41] C. Nayak and F. Wilczek, *Nucl. Phys. B* **417**, 359 (1994).
- [42] A. Houghton, H.-J. Kwon, J. B. Marston and R. Shankar, *J. Phys.: Condens. Matter* **6**, 4909 (1994).
- [43] C. Castellani, S. Caprara, C. Di Castro and A. Maccarone, *Nucl. Phys. B* **594**, 747 (2001).
- [44] T. Maskawa and H. Nakajima, *Prog. Theor. Phys.* **52**, 1326 (1974).
- [45] P. I. Fomin and V. A. Miransky, *Phys. Lett.* **64B**, 166 (1976).
- [46] R. Fukuda and T. Kugo, *Nucl. Phys. B* **117**, 250 (1976).
- [47] V. A. Miransky, *Nuovo Cimento* **90A**, 149 (1985); *Sov. Phys. JETP* **61**, 905 (1985).
- [48] V. P. Gusynin, *Mod. Phys. Lett. A* **5**, 133 (1990).
- [49] K.-I. Kondo and H. Nakatani, *Nucl. Phys. B* **351**, 236 (1991).
- [50] D. Atkinson, H. J. De Groot and P. W. Johnson, *Int. J. Mod. Phys. A* **7**, 7629 (1992).
- [51] K.-I. Kondo, H. Mino and H. Nakatani, *Mod. Phys. Lett. A* **7**, 1509 (1992).
- [52] Z. K. Liu, J. Jiang, B. Zhou, Z. J. Wang, Y. Zhang, H. M. Weng, D. Prabhakaran, S.-K. Mo, H. Peng, P. Dudin, T. Kim, M. Hoesch, Z. Fang, X. Dai, Z. X. Shen, D. L. Feng, Z. Hussain, and Y. L. Chen, *Nature Mat.* **13**, 677 (2014).
- [53] This reduction does not compromise anyhow the linear character of the dispersion in all three dimensions, which is an essential feature of our model since otherwise the scaling rules and critical behavior could change drastically as shown in B.-J. Yang, E.-G. Moon, H. Isobe and N. Nagaosa, *Nature Phys.* **10**, 774 (2014).
- [54] C. Zhang, Z. Yuan, S. Xu, Z. Lin, B. Tong, M. Z. Hasan, J. Wang, C. Zhang, S. Jia, report arXiv:1502.00251.